tween $\Delta\mu$ and T_K/T_g is assumed, observed correlations between the empirical NM parameters x and Δh^* and the KWW parameter β are correctly predicted. A correlation between Δh^* and β is also observed for polymers in the rubbery state above T_g, where relaxation is linear (*17*), and is consistent with the correlation between the same parameters observed under the nonlinear conditions prevailing below T_g. The ratio T_K/T_g is a measure of fragility in Angell's classification scheme for liquids (*17*, *18*), implying that more fragile liquids produce more nonlinear glasses. This is borne out by the correlations between the NM and KWW parameters being consistent with the fragility classification scheme.

The description and prediction of physical aging effects is fraught with difficulties caused by the complexity of their nonlinear and nonexponential character. The problem is acute for polymers because of the coupling between aging and the dynamic and thermodynamic properties that are important in their applications. The current phenomenologies for purely thermal histories are adequate for many engineering applications, such as those for inorganic glasses, for example (*3*), but fail for glasses that are very far from equilibrium. The reasons for this failure are not known with certainty, although the handling of nonlinearity, or the methods for combining nonlinearity and nonexponentiality, or both are suspected by some (*5*, *7*, *8*). A generally accepted methodology for treating nonthermal perturbations to polymers has not yet been developed. Theoretical understanding of the glass transition, upon which a better understanding of physical aging will presumably be based, is at present too poorly developed to be of much help. New approaches to these long-standing problems are sorely needed.

REFERENCES AND NOTES

1. L. C. E. Struik, *Physical Aging in Amorphous Polymers and Other Materials* (Elsevier, Amsterdam, 1978).
2. D. J. Plazek and G. C. Berry, in *Glass: Science and Technology*, D. R. Uhlmann and N. J. Kreidl, Eds. (Academic, Orlando, FL, 1986), vol. 3, p. 363.
3. G. W. Scherer, *Relaxation in Glass and Composites*, (Wiley, New York, 1986).
4. S. Matsuoka, *Relaxation Phenomena in Polymers* (Hanser, New York, 1992).
5. I. M. Hodge, *J. Non-Cryst. Solids* **169**, 211 (1994).
6. C. Arnold-McKenna and G. B. McKenna, *J. Res. Natl. Inst. Stand. Technol.* **98**, 523 (1993).
7. K. L. Ngai and G. B. Wright, Eds. *J. Non-Cryst. Solids* **131–133** (1991).
8. K. L. Ngai, E. Riande, G. B. Wright, Eds., *ibid.* **172–174** (1994).
9. A possible vertical shift due to a change in the dispersion of the compliance function with aging is small for these data.
10. It is customary to refer to τ as a relaxation time, although one should strictly speak of a retardation time for compliance functions.
11. A. K. Doolittle and D. B. Doolittle, *J. Appl. Phys.* **28**, 1673 (1957); M. L. Williams, R. F. Landell, J. D. Ferry, *J. Am. Chem. Soc.* **77**, 3701 (1955); G. Adam and J. H. Gibbs, *J. Chem. Phys.* **43**, 139 (1965).
12. A. J. Kovacs, *Fortschr. Hochpolym. Forsch.* **3**, 394 (1963); A. J. Kovacs *et al.*, *J. Polym. Sci.* **17**, 1097 (1979); J. M. Hutchinson and A. J. Kovacs, *J. Polym. Sci. Phys.* **14**, 1575 (1976).
13. O. S. Narayanaswamy, *J. Am. Ceram. Soc.* **54**, 491 (1971); C. T. Moynihan *et al.*, *ibid.* **59**, 12 (1976).
14. B. E. Read *et al.*, *Polymer* **33**, 2689 (1992); A. F. Yee *et al.*, *J. Polym. Sci. Polym. Phys.* **26**, 2463 (1988); G. C. Stevens and M. J. Richardson, *Polymer Commun.* **26**, 77 (1985).
15. Tensile stresses and the accompanying strains (ε) produce an increase in volume V in materials with a Poisson ratio (ν) less than 0.5: $\Delta V/V \approx \varepsilon(1 - 2\nu)$. The corresponding increases in v_f and S_c decrease τ.
16. G. W. Scherer, *J. Am. Ceram. Soc.* **67**, 504 (1984); I. M. Hodge, *Macromolecules* **20**, 2897 (1987); *J. Non-Cryst. Solids* **131–133**, 435 (1991).
17. K. L. Ngai and R. W. Rendell, *The Physics of Non-Crystalline Solids*, L. D. Pye, W. A. LaCourse, H. J. Stevens, Eds. (Taylor and Francis, London, 1992), p. 309; D. J. Plazek and K. L. Ngai, *Macromolecules* **24**, 1222 (1991).
18. R. Bohmer and C. A. Angell, *Phys. Rev. B* **45**, 10091 (1992); *ibid.* **48**, 5857 (1993); R. Bohmer *et al.*, *J. Phys. Chem.* **99**, 4201 (1993).

19. It is a pleasure to thank J. M. O'Reilly for valuable discussions.

Metallic Glasses

A. Lindsay Greer

Amorphous metallic alloys, relative newcomers to the world of glasses, have properties that are unusual for solid metals. The metallic glasses, which exist in a very wide variety of compositions, combine fundamental interest with practical applications. They also serve as precursors for exciting new nanocrystalline materials. Their magnetic (soft and hard) and mechanical properties are of particular interest.

Materials with each of the major bonding types (ionic, covalent, van der Waals, hydrogen, and metallic) can be obtained in amorphous (that is, noncrystalline) solid forms. Metallic amorphous materials are comparative newcomers to this group. They first came to prominence with Duwez's demonstration in 1959 that an amorphous $Au_{75}Si_{25}$ alloy (the composition is given here, as throughout this article, in atomic percent) could be obtained by rapid cooling of the liquid (*1*). Formed when the liquid becomes increasingly viscous on cooling and fails to crystallize, such a material can correctly be termed a glass. Metallic glasses are but a subset of a range of metallic amorphous solids that can be made by a wide variety of techniques. Undoubtedly, amorphous metallic materials had been made, and even recognized as such, before Duwez's experiments; an example is early work on the condensation of thin films on substrates at liquid helium temperatures (*2*). The significance of Duwez's work, seen more clearly when the improved cooling technique of melt-spinning was developed (Fig. 1), was that vitrification of a liquid permits comparatively large quantities of an alloy to be made into the amorphous state, certainly much more than could be made by thin-film techniques.

In addition to their fundamental interest, metallic glasses were soon realized to have considerable commercial importance when iron-based compositions were found to have excellent soft magnetic properties (*3*). With their ready availability, fundamental interest, and properties of technological importance, metallic glasses in the late 1970s and 1980s were the focus of an explosion of academic and industrial research. Some years on, the novelty has faded. Some commercial applications are well established, and others are still awaited. Yet research on metallic glasses remains active, not least because of continuing discoveries that open up new possibilities. This article considers the current state of the field and focuses on recent developments. Further background material may be found, for example, in (*4*, *5*).

The author is in the Department of Materials Science & Metallurgy, University of Cambridge, Pembroke Street, Cambridge CB2 3QZ, United Kingdom.

How to Make a Metallic Glass

A glass is made if a liquid is cooled sufficiently rapidly to avoid crystallization. With conventional oxide glasses, the critical cooling rate is so low that it is not an important production parameter. For metallic glasses, however, critical cooling rates are usually rather high. Melt-spinning (Fig. 1) has been the main technique for metallic glass production, and it gives cooling rates of the order of 10^5 to 10^6 K s^{-1}. There are, of course, many other techniques for rapidly cooling an alloy liquid. For example, a jet of molten alloy can be ejected into a stream of water to produce wire, or (in any of the many variants of atomization) broken up to produce droplets. With such techniques, the cooling rate is comparable to that in melt-spinning and the interest is in the forms of the product. A contrasting example is pulsed laser quenching, in which a very thin (~100 nm) surface layer is melted by an incident beam of duration as short as a few picoseconds. The thin layer on top of a large cold substrate experiences ultrarapid cooling, as fast as 10^{14} K s^{-1} (*6*).

Even when the critical cooling rate is not so high as to require a technique such as melt-spinning, it may still be necessary to cool a liquid under very clean conditions to avoid crystallization in contact with nucleants. Techniques for achieving cleanliness include encapsulation of the liquid alloy in another liquid (the emulsion technique and fluxing) or containerless solidification in free fall.

Techniques used for making amorphous alloys are listed in Table 1. Apart from cooling the liquid, there are many other methods. Techniques based on deposition from the vapor (evaporation or sputtering) or from solution (electrodeposition or electroless deposition) can be considered akin to rapid liquid quenching in that a solid is formed when the mobility of the atoms is rapidly decreased. There are also many techniques based on the formation of an amorphous phase within the solid state. Irradiation by ions or high-energy electrons can destroy crystalline order in a single-phase solid, as can heavy mechanical work (for example, by grinding). Alloying can be achieved in the solid state by ion implantation, ion mixing, or mechanical alloying, and each of these techniques can yield an amorphous product. In all of these solid-state techniques, considerable energy is supplied, and the introduction of defects and ultimate amorphization may not be a surprise. For example, the collision cascades that occur after ion bombardment can be likened to liquidlike volumes that are then rapidly quenched.

There are other techniques for producing an amorphous phase in which the only input of energy is thermal annealing. As was first demonstrated and explained by Schwarz and Johnson (*7*), certain combinations of crystalline elemental metals react in the solid state to produce an amorphous phase. A further type of amorphization, rarely observed, is the transformation of a supersaturated solid solution. These transformations are discussed further below.

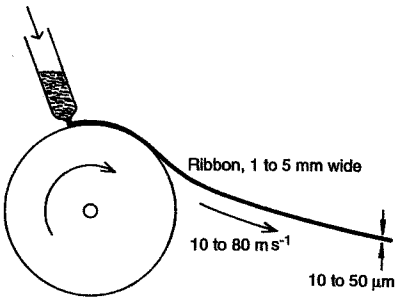

Fig. 1. The most common laboratory technique for producing metallic glasses is melt-spinning (*54*), shown here schematically, in which the molten alloy is ejected onto the flat rim of a rapidly rotating wheel (typically copper) to produce a thin ribbon up to a few millimeters wide. In the related industrial process of planar flow casting (*55*), proximity of the ejection nozzle to the wheel gives tight control of ribbon dimensions, and widths up to a few tens of centimeters can be produced.

Compositions of Metallic Glasses

The composition ranges of alloys that can be made glassy of course depend on the production method. If the cooling rate of the liquid is more rapid, glass formation ranges are widened. However, the composition ranges made glassy or amorphous by different techniques do not vary enormously. The general types of alloy emerging as glass formers (for example, by melt-spinning) are listed in Table 2.

How are the compositions in Table 2 to be understood? Various criteria have been proposed for glass formation. Crystallization of the liquid can occur only below the liquidus temperature T_m, and glass formation is assured if the still-uncrystallized liquid is cooled to the underlying glass transition temperature T_g. Thus glass formation is expected to be easiest when the interval between the liquidus and the glass transition is minimal. The reduced glass transition temperature T_g/T_m is a useful guide to glass-forming ability. Because T_m can be a strong function of composition, but T_g usually is not, glass formation is expected near deep depressions (eutectics) in the liquidus; this prediction is substantially verified experimentally (Fig. 2). Essentially the glass-forming compositions are those at which the liquid is relatively stable compared to the crystalline phases. Solutes generally stabilize the liquid (through entropy) but destabilize the elemental solid solutions through the difficulty of incorporating foreign atoms in the crystal structures. The difficulty of incorporation is related to the sizes of the atoms (*8*). No metallic glass is known based on components that have a difference in atomic diameter <10% (*9*).

It is clear from Table 2 that all major categories of metal are represented. However, it has been clear that some elements (palladium and iron are prominent examples) lend themselves to glass formation more easily than others. Aluminum, important for its low density and aerospace applications, is an example of a metal that is very difficult to incorporate as the dominant element in metallic glasses. Work in France (*10*) and Japan (*11*) led to the development of alloys with gradually increasing aluminum content. The significant breakthrough, the production of glasses that contain >80 atomic % Al and that are ductile, came in 1988 through independent work in the United States (*12*) and Japan (*13*). The new alloys are of the type Al-TM-Ln (where TM represents a transition metal and Ln a lanthanide) such as $Al_{90}Fe_5Ce_5$ (*12*) and $Al_{85}Ni_{10}Y_5$ (*13*). They have excited interest in metallic glasses based on light metals and have proved to be the basis for further significant developments in ultrafine-scale crystallized materials (described below).

Confusion Reigns

For some time, alloy compositions have been known that do not require rapid liquid cooling for glass formation. An example is $Pd_{40}Ni_{40}P_{20}$, for which sections 10-mm thick can be made glassy by cooling at <1 K s^{-1} under very clean conditions (*14*). The noble metal palladium, although often found in glass-forming compositions, is unlikely to be widely applied because of its expense. Interest increased when Inoue and co-workers (*15*, *16*) discovered further alloy types with similar glass-forming ability, sometimes not even requiring any special precautions with cleanliness. Some easy glass formers are Ln-Al-TM alloys, such as $La_{55}Al_{25}Ni_{20}$, and Mg-TM-Ln alloys, such as $Mg_{65}Cu_{25}Y_{10}$ (*15*, *16*). Significantly, it was also found that lanthanides are not necessary, as in the Zr-Al-TM family (*17*). The ability to form metallic glasses very easily, in large cross-sections, from common elements has naturally aroused much interest and led to rapid development. In particular,

Table 1. Some production methods for glassy and amorphous metals.

Method	Ref.
Rapid liquid cooling	
Melt-spinning, planar flow casting	(*54*, *55*)
Atomization	(*56*, *57*)
Wire formation in water	(*58*)
As a surface treatment	
Scanned laser or electron beam	(*59*, *60*)
Pulsed laser beam	(*6*)
Undercooling of clean liquids	
Emulsion technique	(*61*)
Fluxing	(*62*)
Solidification in free fall	(*63*)
Physical vapor deposition	
Evaporation	(*2*)
Sputtering	(*64*)
Chemical methods	
Electroless deposition	(*65*)
Electrodeposition	(*66*)
Precipitation	(*67*)
Hydrogenation	(*68*)
Irradiation	
By light or heavy ions	(*69*, *70*)
By electrons	(*71*)
By neutrons	(*72*)
Ion implantation	(*73*)
Ion mixing	(*74*)
Mechanical methods	
Grinding	(*75*)
Mechanical alloying	(*76*)
Reactions	
Solid-state reaction of elements	(*7*)
Decomposition of crystalline solid solution	(*30*)

the general rule of stabilizing the liquid to promote glass formation has been exploited by adding more components. This is in effect applying a "confusion principle," in which the diverse components present, in particular their different sizes, inhibit crystallization. Work in Japan and the United States has led to many new compositions, such as $Zr_{41.2}Ti_{13.8}Cu_{12.5}Ni_{10.0}Be_{22.5}$ (*18*, *19*). These are based on a mixture of early transition metals, a mixture of late transition metals, and possibly also beryllium, chosen because of its small atomic size. Alloys such as these have been cast as cylinders up to 16 mm in diameter, and there is no reason to suppose that this is an upper limit. As can be seen in Fig. 3 the glass-forming ability of such compositions approaches that of the traditional oxide glasses.

Do Metals Form True Glasses?

The archetypal glasses are those of the oxides, particularly those based on silica. The basic model for their structure is the continuous random network, in which bonding of nearest neighbors is the same as that in the crystal but longer range order is absent. Such glasses have associated with them particular properties. In contrast to these more familiar glasses, metallic glasses typically are much less stable. On heating they crystallize, and this process inhibits observation of the properties generally associated with the glassy state, such as rapid viscous flow at and above T_g. The compositions listed in Table 2 have been determined to be amorphous by x-ray or electron diffraction. Yet, as will be shown below, such evidence may be inconclusive, and there has been a recurring question of whether the materials obtained are really amorphous or microcrystalline. Even if they are amorphous, there is the further question of whether they can truly be regarded as glasses formed continuously from the liquid. Silicon provides an example illustrating that glasses and amorphous materials are not always the same (*20*). Liquid silicon has a high density and is metallic. Normal crystalline silicon has tetrahedral covalent bonding. Amorphous silicon, which can be made by deposition as well as by solidification from the liquid, also has a local tetrahedral coordination with tetrahedral bonding. In its bonding type, solid amorphous silicon is therefore quite distinct from the liquid and cannot be regarded as a glass, which if formed would be dense and metallic.

Notwithstanding the problems with lack of stability, there are many indications that metallic glasses are true glasses. On annealing, their properties change in a way characteristic of the structural relaxation of conventional glasses (*21*). This relaxation is not a precursor to crystallization (some of the property changes are opposite in sign to those expected for crystallization), but brings the structure of the glass closer to that of the equilibrium liquid at the annealing temperature. By successive annealing at different temperatures, reversible changes can be observed. For metallic glasses that are normally made by rapid cooling, the initial state is highly unrelaxed, and annealing predominantly leads to densification. Even though crystallization precludes prolonged experiments, viscosity and specific heat changes near T_g are as expected for real glasses. It has recently become possible to demonstrate all such effects more convincingly by using the new very stable, multicomponent glasses described above. In these materials, rapid crystallization occurs at temperatures that can be more than 100 K higher than T_g (*19*). This situation gives plenty of opportunity for measurements around the glass transition, where the properties are particularly characteristic of the glassy state. As an example, these new materials show the capability for superplastic deformation associated with the archetypal oxide glasses. Also, and most importantly, the easy glass-forming compositions do permit some measurements (particularly thermal) to be made continuously (without intervening crystallization) between the glassy state and the liquid, thus directly demonstrating the link between them (*22*).

In addition to relaxation effects, crystallization (or "devitrification") itself provides further evidence for the glassy state. When crystallization occurs on heating a metallic glass, microstructural studies show that it involves nucleation and growth, just as for

Table 2. Examples of glass-forming alloys. All compositions are quoted in atomic percent. The amorphous alloys have been formed by a variety of techniques, mostly rapid liquid-quenching. This is far from a comprehensive list; only some representative alloys and compositions are given in each category. For binary alloys, however, some indication is given of glass-forming ranges.

Alloy	Glass-forming range	Ref.
Late transition metal–metalloid		
$Fe_{100-x}B_x$	x = 12–25	(*77*)
$Pd_{100-x}Si_x$	x = 14–22	(*78*)
$Fe_{40}Ni_{40}B_{20}$		(*79*)
$Fe_{40}Ni_{40}P_{14}B_6$		(*80*)
Early transition metal–metalloid		
$Ti_{100-x}Si_x$	x = 15–20	(*81*)
$W_{60}Ir_{20}B_{20}$		(*82*)
Early transition metal–late transition metal		
$Nb_{100-x}Ni_x$	x = 40–70	(*83*)
$Cu_{100-x}Zr_x$	x = 25–60	(*84*)
$Ni_{100-x}Zr_x$	x = 10–12, 33–80	(*85*, *86*)
$Zr_{60}Ni_{25}Al_{15}$		(*87*)
Aluminum-based		
$Al_{100-x}La_x$	x = 10, 50–80	(*88*)
$Al_{83}Cu_{15}V_7$		(*89*)
$Al_{85}Ni_{10}Zr_5$		(*36*)
$Al_{90}Fe_5Ce_5$		(*12*)
$Al_{80}Ni_{10}Y_{10}$		(*13*)
Lanthanide-based		
$La_{100-x}Au_x$	x = 18–26	(*90*)
$Gd_{100-x}Fe_x$	x = 32–50	(*91*)
$La_{55}Al_{25}Ni_{20}$		(*92*)
Alkaline-earth–based		
$Mg_{100-x}Zn_x$	x = 25–32	(*93*)
$Ca_{100-x}Al_x$	x = 12.5–47.5	(*94*)
$Mg_{65}Cu_{25}Y_{10}$		(*95*)
$Be_{40}Zr_{10}Ti_{50}$		(*96*)
Actinide-based		
$U_{100-x}Co_x$	x = 24–40	(*97*)

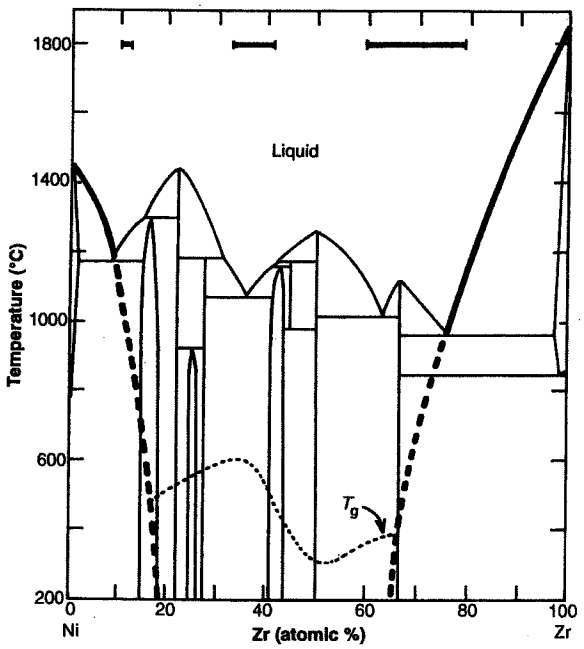

Fig. 2. The phase diagram of the Ni-Zr system. Glass formation (by melt-spinning), shown by the horizontal bars, is found near eutectic compositions, where the gap between T_m and T_g (dotted line) is minimized (*85*, *86*). The heavy lines, solid and dashed, indicate T_m and its metastable extension for each elemental solid solution. Solid-state amorphization by reaction of the elements occurs between the metastable extensions and below T_g (*100*).

solidification of a liquid and crystallization of conventional oxide glasses (*23*). Thus, for most or all of the compositions in Table 2, there is firm evidence that the materials are glassy. In addition, all comparisons of property measurements on alloy compositions made into glasses by rapid cooling of the liquid and made amorphous by other techniques suggest that the materials are similar. Strong evidence on this point is provided by thermodynamic measurements.

Thermodynamics of Glasses and Amorphous Alloys

The thermodynamic properties of a glass can be estimated by extrapolating to lower temperatures the properties of the liquid. In performing such an extrapolation, it is important to note that glass-forming liquids have specific heats significantly greater (perhaps as much as two times greater, just above T_g) than the corresponding crystalline solids. Specific heats can be measured directly in undercooled liquids or can be estimated from the heat of crystallization of a glass (*24*, *25*). In addition, there are some electrochemical measurements of the thermodynamics of the glassy state itself (*26*). Estimates of the Gibbs free energy of glassy phases have proved useful in interpreting amorphous-phase formation by solid-state reactions (*27*). In such a reaction at interfaces between thin films of the elements, nucleation of the stable intermetallic compounds appears to be stifled. The relevant phase equilibria then involve only the liquid or glassy phase and the elemental solid solutions. These equilibria are indicated by the heavy lines in Fig. 2. This metastable phase diagram shows that the formation of the amorphous phase on annealing at 200° to 300°C can be simply considered to be a eutectic melting occurring below T_g (*28*).

A still more striking example of the use of glassy-state thermodynamics to interpret a solid-state amorphization phenomenon is that of inverse melting. The supersaturated body-centered-cubic (bcc) solid solution of $Cr_{55}Ti_{45}$, when annealed at 550°C, transforms to an amorphous phase of the same composition. However, the bcc phase itself forms on cooling the liquid. Thus, if the amorphous phase is indeed continuous with the liquid, its free energy must equal that of the bcc phase at *two* temperatures (*29*). This behavior, calculated from thermodynamic parameters of the system by Bormann (*30*), is illustrated in Fig. 4. At the higher equilibrium temperature is the normal melting point. At the lower equilibrium temperature is a novel inverse melting point, at which a crystal would melt on cooling. Such melting must mean that the liquid or amorphous phase at this point has a lower entropy than the crystal; this remarkable result may be associated with the obvious positional entropy difference between the amorphous and crystalline phases being outweighed by greater chemical order in the former. However, the key point is that the appearance of the amorphous phase can be explained from the ordinary thermodynamics of the alloy system by extrapolating the liquid properties to lower temperatures.

Glasses, Nanocrystals, and Quasicrystals

There have been many attempts to model the structure of amorphous metallic alloys. Early on it became clear that simple models based on microcrystalline aggregates had significant problems, and that the most successful models were based on dense random packing (which can be regarded as the counterpart of the continuous random network for metallic rather than covalent bonding). From the above discussions of properties and thermodynamics, it may appear that there is no doubt about the existence of the metallic glassy state. Yet work on deposited thin films has reopened the amorphous versus microcrystalline question. For example, thin-film $Al_{83}Mn_{17}$ appears amorphous in electron diffraction and imaging, but when it is annealed it transforms to a polycrystalline material by what appears (by calorimetry and microstructural observation) to be a continuous process of grain growth (*31*). Thus it appears to be initially in a nanocrystalline state. On the other hand, there are many compositions, including many based on aluminum, that appear by the same calorimetric and microstructural tests to be truly amorphous (*32*, *33*).

In examining this question, the structures of alloys which are more obviously in a glassy state can be considered first. Basic analyses of radial distribution functions show average coordination numbers in the range 11.5 to 14.5, values consistent with extrapolations from metallic liquids. However, analysis of partial pair distribution functions show that there can be strong chemical ordering. For example, in alloys such as $Ni_{81}B_{19}$ there appear to be no B–B nearest neighbors (*34*). Models based on the dense random network have been refined by increasing the degree of local order. It appears that not only can there be considerable chemical order, but that local coordinations can be similar to those in crystalline compounds. Currently a model based on nanoscale twinning ("chemical twinning") appears to be quite successful in fitting experimental data (*35*). There are no boundaries in this model, so it supports the concept of an amorphous rather than a microcrystalline state.

However, such a model is successful with some "amorphous" alloys and not others. In particular, it is not successful for at least some of the Al-based alloys (*36*) that "de-

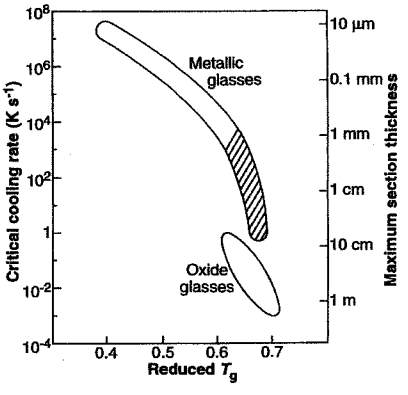

Fig. 3. The glass-forming ability of alloys and oxides are compared. The critical cooling rate for glass formation varies strongly with the reduced T_g and gives an approximate maximum section thickness. The shaded area corresponds to the alloys such as Ln-Al-TM (*15*), Mg-TM-Ln (*16*), Zr-Al-TM (*17*, *18*), Zr-TM-Be (*19*) (TM, transition metal, and Ln, lanthanide). [Adapted from (*19*) with permission from Elsevier Science S.A., Lausanne, Switzerland]

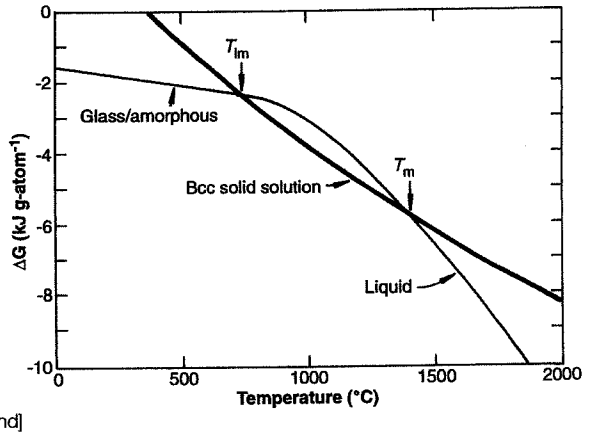

Fig. 4. Calculated Gibbs free energies (relative to hexagonal close-packed Ti and bcc Cr) of the bcc solid solution and of the liquid-glassy phase in $Cr_{55}Ti_{45}$ (atomic percent). Indicated for congruent transformations between these phases are the normal melting point T_m and a novel inverse melting point T_{lm} (which is at or below T_g). On annealing the bcc solid solution below T_{lm} (for example, at 550°C), it amorphizes, as predicted. [Adapted from (*30*) with permission from Elsevier Science S.A., Lausanne, Switzerland]

vitrify" to a quasicrystalline phase with icosahedral symmetry (of which the thin-film $Al_{83}Mn_{17}$ cited above is an example). Aluminum is one of the main base elements for quasicrystalline phases. Thus it may be that some apparently amorphous alloys are really aggregates of nanoscale quasicrystalline grains. Much further work is clearly needed to explore the distinction between such materials, true amorphous phases, and true nanocrystalline phases formed by other techniques.

Properties and Applications

Metallic glasses are indeed metallic in their electrical conduction, but they can have very high resistivities. The temperature dependence of resistivity can be positive or negative and is in any case close to zero, which may lead to some potential applications (*37*). Their mechanical properties, because of the absence of crystal slip, are quite unlike those of conventional metals. At high temperatures, there is viscous flow, which opens up the possibility of superplastic forming. At ambient temperature, although some metallic glasses are brittle, many are not. However, the plastic flow is concentrated into shear bands, which indicates that any flow leads to softening, not hardening, as normally expected for metals (*38*). This work-softening unfortunately means that, in tension, a metallic glass sample fails with little plastic elongation, in an apparently brittle manner. The absence of crystal-slip mechanisms leads to very high flow stresses. For example (Fig. 5), an aluminum-based glass can have a flow stress as high as 1250 MPa (*39*), about twice as high as the best precipitation-hardened conventional alloy and certainly immensely harder than the commercial purity element (~200 MPa). Despite the high strengths, there has been only limited interest (for example, as reinforcing fibers in auto tires) in metallic glass ribbons for mechanical applications (*40*); this is partly because their properties, although good for alloys, are not outstanding compared to other fibers, and partly because of the lack of fatigue resistance and the apparent brittleness caused by the work-softening. A mechanical property that is exploited is wear resistance (*41*). With combined wear and corrosion resistance, metallic glass coatings are suitable to withstand aggressive environments such as are found in valves. In combination with their soft magnetic properties (see below), the wear resistance is useful in tape recorder heads. The capability of amorphous alloys to be more ductile than their crystalline counterparts in bending has led to significant application as brazing foils (*42*).

The corrosion resistance, although not necessarily good, can be outstanding—promoted by the chemical and structural homogeneity of metallic glasses and by the ability to have high levels of solute to produce protective oxides (*43*). Protective coatings can of course be deposited by a variety of methods, but they may also be made in situ by rapid solidification of a thin surface layer melted by a scanned laser or electron beam. With such "laser glazing," it is difficult to get uniform completely amorphous coatings, but surface coatings of this kind have nevertheless attracted wide interest. Another chemical property of interest is the use of amorphous alloys as catalysts (*40*).

Of all of the properties of metallic glasses, it is their soft magnetism that has led to the most significant applications. The microstructural homogeneity of the glasses and the absence of magnetocrystalline anisotropy can give very low coercivity and low hysteretic losses. On the other hand, strong magnetostriction in many compositions and low saturation magnetizations (because of high solute levels) can be disadvantages. There is now large-scale production, by planar-flow casting, of iron-based soft magnetic material for the cores of distribution transformers, and there are many other applications in small magnetic devices (*3*).

Because of the requirement (for most compositions) for rapid liquid quenching, metallic glass samples are available only in thin cross sections. The tendency to crystallize impedes efforts to make bulk products by consolidating powder or chopped ribbon. However, the forms available, such as ribbons or sheet, can be quite suitable for many applications. For example, ribbons can be used for reinforcing elements, and thin sheet can be used for transformer core laminations or magnetic shielding.

Devitrification

Conventional oxide glasses are of interest not only in themselves but also because they are the precursors of useful glass-ceramics, obtained by crystallization of the glass, that is, by devitrification. The focus of this article so far has been on metallic glasses themselves and has reflected the common view that devitrification (either through the production route not yielding a fully glassy state, or through subsequent annealing) is undesirable. Where metallic glasses have novel properties, devitrification can be expected to destroy those properties; for example, devitrification increases the coercivity in soft

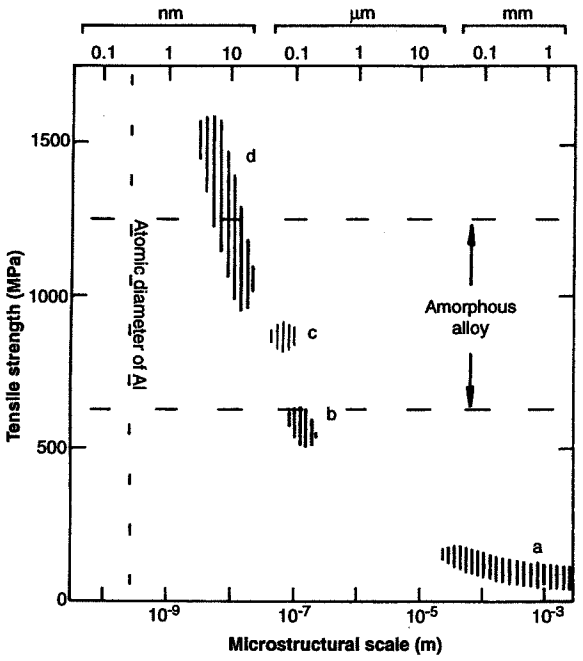

Fig. 5. The tensile strengths of aluminum alloys compared as a function of microstructural scale: (a) commercial purity aluminum; (b) the strongest conventional precipitation-hardened Al alloys; (c) amorphous, or part amorphous, Al-TM-Ln alloys, consolidated and crystallized (*53, 101*); and (d) amorphous Al-TM-Ln alloys, partially devitrified (either during quenching or by annealing) to give nanometer-scale crystallites (*51, 52, 102*). The diameter of an Al atom and the wide range of tensile strengths for fully amorphous Al-TM-Ln alloys (*39, 51, 102*) are shown for comparison (TM, transition metal, and Ln, lanthanide).

Table 3. Property enhancements through devitrification.

Property	Ref.
Mechanical properties	
Increased ductility	(*98*)
Increased flow stress and fracture strength	(*50, 51*)
Superplasticity	(*53*)
Soft magnetic properties	
Low coercivity	(*48, 49*)
High saturation magnetization	(*48, 49*)
Reduced high-frequency losses	(*44*)
Stress-induced anisotropy	(*45*)
Hard magnetic properties	(*47*)
Increased critical current in type II superconductors	(*99*)

magnetic glasses. On the other hand, it has gradually been realized that fully or partially crystalline materials made from metallic glasses can have useful properties (Table 3), and important recent work is in this field. Slight devitrification is useful in tailoring properties. A fine dispersion of crystals in a ferromagnetic glass can pin domain boundaries and reduce hysteretic losses at high frequency (*44*). Surface devitrification can induce stresses to change the magnetic anisotropy (*45*). More surprising is that substantial or even complete devitrification can produce interesting materials. At first glance it seems perverse to adopt a difficult production route to avoid crystallization and make glass, only then to crystallize the glass. The key point is that any crystalline product made from a glass has a very fine and very uniform microstructure. The uniformity follows from the chemical uniformity of the glass, which formed from the liquid without segregation. The fine scale of the microstructure arises because devitrification is effectively the solidification of the liquid at very high undercooling; crystal nucleation is favored, and growth is inhibited.

Although there were some early claims of useful tool steels (*46*), the first major application of a devitrified alloy was the hard magnetic material based on the phase $Fe_{14}Nd_2B$ (*47*). Large-scale commercial production of this material by rapid solidification commenced very shortly after it was discovered. In fact, the material can be made by a variety of routes, but these include devitrifying an initially glassy material and the closely related route of quenching not quite sufficiently fast to obtain a fully glassy product. That a material with a fine grain size should have hard magnetic properties is not surprising. Much more intriguing is the observation that a soft magnetic metallic glass can partially crystallize to a material that has good or even improved soft magnetic properties. Such materials, first discovered in Japan, have been widely studied. Initial compositions were of the type $Fe_{73.5}Cu_1Nb_3Si_{13.5}B_9$ (*48*), but more recently compositions of the kind of $Fe_{91}Zr_7B_2$ (*49*) have shown good properties while having a greater concentration of magnetic species. These materials consist of a dispersion of fine (10 to 20-nm diameter) crystallites in a amorphous matrix. The fine scale precludes effective pinning of domain boundaries.

A more recent example of spectacular improvements found in a partially crystalline material are the mechanical properties of Al-TM-Ln alloys. The materials, developed separately in Japan (*50*) and the United States (*51*), consist of 3- to 10-nm diameter crystallites of cubic close-packed aluminum embedded in an amorphous matrix and have optimum strength for a crystalline volume fraction of ~25%. They are obtained by quenching at below the critical rate or by annealing an initially amorphous material. The devitrification can also be induced by mechanical working. The most remarkable feature of these materials is their ultrahigh tensile fracture strength [as high as 1560 MPa for $Al_{88}Ni_9Ce_2Fe_1$ (*52*)], combined with their lack of brittleness. This property is illustrated in Fig. 5; the fracture strength of the partially crystalline materials can be as much as 50% greater than that of the corresponding fully amorphous alloy. The reasons for this enhancement are not yet clear. However, the aluminum crystals appear to be too small to contain any dislocations. The potential importance of these novel nanophase composites can be shown on a property chart for engineering materials (Fig. 6). The best of the new alloys have properties well outside the range associated with conventional Al alloys; they have properties in the range of engineering ceramics such as MgO, yet are also ductile.

If partially crystalline materials are of interest, then some degree of devitrification may be permissible during consolidation of amorphous ribbon. Consolidated product, either partially or fully crystalline, has been found to retain a fine-scale microstructure of interest. For example, a consolidated alloy of the Al-TM-Ln type has shown superplastic elongations of >500% at strain rates as high as 1 s^{-1} (*53*). Even after consolidation and deformation, the mechanical properties (for example, a tensile strength ≈900 MPa) are superior to those of conventional commercial high-strength aluminum alloys.

Outlook

The recent developments of aluminum-based glasses with good properties and of the very easy glass-forming alloys have attracted wide interest. They suggest that the research emphasis has firmly shifted from concentration on techniques for metallic glass formation to the exploration for new compositions. For commercial applications, the production technique should be straightforward, and the glasses produced should be stable. In these respects, the use of multicomponent compositions has proved very fruitful and, as most of these systems are unexplored, may yet lead to further surprises. There is no reason to suppose that all significant glass-forming compositions have been discovered.

The advent of a range of very easy glass-forming alloys has established that metals can be made into true glasses and is permitting fundamental work on the metallic glassy state. In addition, it has opened up possibilities for the shaping of metals through viscous flow at elevated temperature, as is used for conventional glasses. This capability could be exploited not only for large-scale sheet forming but for the manufacture of ultrasmall components in which the grain structure of a normal polycrystalline metal would interfere with the shaping (*19*).

Again following belatedly in the footsteps of conventional oxide glasses, it is now clear that metallic glasses can be useful precursors for partially or fully crystalline materials that can have superior properties to the glasses themselves. The products of devitrification are distinguished by the uniformity and ultrafine scale of their microstructures. So far their potential has been demonstrated for magnetic properties and high strength; further exploitation can be expected.

In materials engineering today, there is

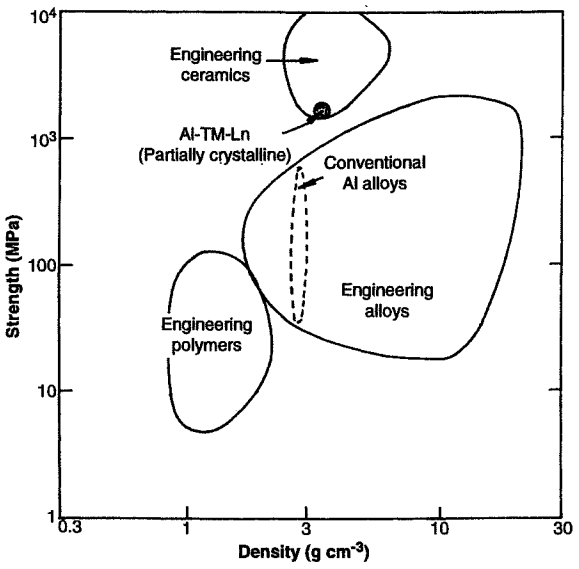

Fig. 6. A strength-density property chart for engineering materials where the application to materials selection is discussed. Amorphous Al-TM-Ln alloys partially crystallized to give a dispersion of nanometer-scale Al crystallites can have properties (*52*) like engineering ceramics and unlike conventional Al alloys. [Adapted from (*103*) with permission from Elsevier Science Ltd., Kidlington, United Kingdom]

much consideration of the replacement of alloys by other materials such as polymers and ceramics. Metallic glasses, and the devitrified materials made from them, represent part of the response of alloys to this. These new metallic materials have a very wide range of novel properties or combinations of properties, ranging from soft or hard magnetism to corrosion resistance and ultrahigh flow stress. They have evolved from laboratory curiosities into materials of industrial application, and research on them has led to improved understanding in many areas, ranging from magnetism to solidification.

REFERENCES AND NOTES

1. K. Klement, R. H. Willens, P. Duwez, *Nature* **187**, 869 (1960).
2. W. Buckel, *Z. Phys.* **138**, 136 (1954).
3. C. H. Smith, in *Rapidly Solidified Alloys: Processes, Structures, Properties, Applications*, H. H. Liebermann, Ed. (Dekker, New York, 1993), pp. 617–663.
4. F. E. Luborsky, Ed., *Amorphous Metallic Alloys* (Butterworths, London, 1983).
5. R. W. Cahn, in *Glasses and Amorphous Materials*, J. Zarzycki, Ed., vol. 9 of *Materials Science & Technology*, R. W. Cahn, P. Haasen, E. J. Kramer, Eds. (VCH Press, Weinheim, 1991), pp. 493–548.
6. C. J. Lin and F. Spaepen, *Acta Metall.* **34**, 1367 (1986).
7. R. B. Schwarz and W. L. Johnson, *Phys. Rev. Lett.* **51**, 415 (1983).
8. T. Egami, Y. Waseda, *J. Non-Cryst. Solids* **64**, 113 (1984).
9. B. C. Giessen, in *Proceedings of the Fourth International Conference on Rapidly Quenched Metals*, T. Masumoto and K. Suzuki, Eds. (Japanese Institute of Metals (JIM), Sendai, 1982), pp. 213–216.
10. J. M. Dubois, G. Le Caer, K. Dehghan, in *Proceedings of the Fifth International Conference on Rapidly Quenched Metals*, S. Steeb and H. Warlimont, Eds. (Elsevier, Amsterdam, 1985), pp. 197–202.
11. A. Inoue and T. Masumoto, in *Encyclopedia of Materials Science and Engineering*, R. W. Cahn, Ed. (Pergamon, Oxford, 1990), suppl. vol. 2, pp. 660–667.
12. Y. He, S. J. Poon, G. J. Shiflet, *Science* **241**, 1640 (1988).
13. A. Inoue, K. Ohtera, A. P. Tsai, T. Masumoto, *Jpn. J. Appl. Phys.* **27**, L280 (1988).
14. A. J. Drehman and A. L. Greer, *Acta Metall.* **32**, 323 (1984).
15. A. Inoue, T. Zhang, T. Masumoto, *Mater. Trans. J.I.M.* **31**, 425 (1990).
16. A. Inoue, T. Nakamura, N. Nishiyama, T. Masumoto, *ibid.* **33**, 937 (1992).
17. T. Zhang, A. Inoue, T. Masumoto, *ibid.* **32**, 1005 (1991).
18. A. Peker and W. L. Johnson, *Appl. Phys. Lett.* **63**, 2342 (1993).
19. T. Masumoto, *Mater. Sci. Eng.*, **A179/A180**, 8 (1994).
20. J. M. Poate, P. S. Peercy, M. O. Thompson, *Mater. Res. Soc. Symp. Proc.* **57**, 465 (1987).
21. A. L. Greer, in *Rapidly Solidified Alloys: Processes, Structures, Properties, Applications*, H. H. Liebermann, Ed. (Dekker, New York, 1993), pp. 269–301.
22. H. W. Kui and D. Turnbull, *Appl. Phys. Lett.* **47**, 796 (1985).
23. U. Köster, *Z. Metallkd.* **75**, 691 (1984).
24. P. V. Evans, A. Garcia Escorial, P. E. Donovan, A. L. Greer, *Mater. Res. Soc. Symp. Proc.* **57**, 239 (1987).
25. L. Battezzati and E. Garrone, *Z. Metallkd.* **76**, 305 (1984).
26. R. Bormann and K. Zöltzer, *Phys. Stat. Sol. (a)* **131**, 691 (1992).
27. R. Bormann, F. Gärtner, K. Zöltzer, *J. Less-Common Met.* **145**, 283 (1988).
28. R. J. Highmore and A. L. Greer, *Nature* **339**, 363 (1989).
29. A. L. Greer, *J. Less-Common Met.* **140**, 327 (1988).
30. R. Bormann, *Mater. Sci. Eng.* **A179/A180**, 31 (1994).
31. L. C. Chen, F. Spaepen, J. L. Robertson, S. C. Moss, K. Hiraga, *J. Mater. Res.* **5**, 1871 (1990).
32. Y. He, H. Chen, G. J. Shiflet, S. J. Poon, *Philos. Mag. Lett.* **61**, 297 (1990).
33. J. C. Holzer and K. F. Kelton, *Acta Metall. Mater.* **39**, 1833 (1991).
34. P. Lamparter, W. Sperl, S. Steeb, J. Blétry, *Z. Naturforsch.* **37a**, 1223 (1982).
35. J. M. Dubois, P. H. Gaskell, G. Le Caer, in *Proceedings of the Fifth International Conference on Rapidly Quenched Metals*, S. Steeb and H. Warlimont, Eds. (Elsevier, Amsterdam, 1985), pp. 567–572.
36. J. M. Dubois, in *Trends in Non-Crystalline Solids*, A. Conde, C. F. Conde, M. Millán, Eds. (World, Singapore, 1992), pp. 343–363.
37. T. Richmond and H. J. Güntherodt, in *Rapidly Solidified Alloys: Processes, Structures, Properties, Applications*, H. H. Liebermann, Ed. (Dekker, New York, 1993), pp. 431–459.
38. F. Spaepen and A. I. Taub, in *Amorphous Metallic Alloys*, F. E. Luborsky, Ed. (Butterworths, London, 1983), pp. 231–256.
39. M. Blank-Bewersdorff, *J. Mater. Sci. Lett.* **10**, 1225 (1991).
40. C. Suryanarayana and F. H. Froes, in *Rapidly Solidified Alloys: Processes, Structures, Properties, Applications*, H. H. Liebermann, Ed. (Dekker, New York, 1993), pp. 737–754.
41. U. Sudarsan, K. Chattopadhyay, Kishore, in *Proceedings of the Fifth International Conference on Rapidly Quenched Metals*, S. Steeb and H. Warlimont, Eds. (Elsevier, Amsterdam, 1985), pp. 1439–1442.
42. A. Rabinkin and H. H. Liebermann, in *Rapidly Solidified Alloys: Processes, Structures, Properties, Applications*, H. H. Liebermann, Ed. (Dekker, New York, 1993), pp. 691–735.
43. M. Janik-Czachor, *Mater. Sci. Eng.* **A179/A180**, 142 (1994).
44. A. Datta, N. J. De Cristofaro, L. A. Davis, in *Proceedings of the Fourth International Conference on Rapidly Quenched Metals*, T. Masumoto and K. Suzuki, Eds. (JIM, Sendai, 1982), pp. 1007–1010.
45. H. N. Ok and A. H. Morrish, *Phys. Rev. B* **23**, 1835 (1981).
46. R. Ray, *Met. Prog.* **121**, 29 (1982).
47. J. J. Croat, J. F. Herbst, R. W. Lee, F. E. Pinkerton, *J. Appl. Phys.* **55**, 2078 (1984).
48. Y. Yoshizawa, S. Oguma, K. Yamauchi, *ibid.* **64**, 6044 (1988).
49. K. Suzuki, N. Kataoka, A. Inoue, T. Masumoto, *Mater. Trans. J.I.M.* **32**, 93 (1991).
50. Y. H. Kim, A. Inoue, T. Masumoto, *ibid.* **31**, 747 (1990).
51. H. Chen, Y. He, G. J. Shiflet, S. J. Poon, *Scr. Metall. Mater.* **25**, 1421 (1991).
52. A. Inoue, Y. Horio, Y. H. Kim, T. Masumoto, *Mater. Trans. J.I.M.* **33**, 669 (1992).
53. K. Higashi, *et al.*, *Scr. Metall. Mater.* **26**, 191 (1992).
54. H. H. Liebermann, *Mater. Sci. Eng.* **43**, 203 (1980).
55. M. C. Narasimhan, U.S. Patent 4 142 571 (1979).
56. S. A. Miller and R. J. Murphy, *Scr. Metall.* **13**, 673 (1979).
57. Y. W. Kim, H. M. Kim, T. F. Kelly, *Acta Metall.* **37**, 247 (1989).
58. M. Hagiwara and A. Inoue, in *Rapidly Solidified Alloys: Processes, Structures, Properties, Applications*, H. H. Liebermann, Ed. (Dekker, New York, 1993), pp. 139–155.
59. E. Schubert and H. W. Bergmann, *ibid.*, pp. 195–230.
60. E. M. Breinan, D. B. Snow, C. O. Brown, B. H. Kear, in *Rapid Solidification Processing, Principles and Technologies II*, R. Mehrabian, B. H. Kear, M. Cohen, Eds. (Claitor's, Baton Rouge, LA, 1980), p. 440.
61. J. H. Perepezko and J. S. Smith, *J. Non-Cryst. Solids* **44**, 65 (1981).
62. H. W. Kui, A. L. Greer, D. Turnbull, *Appl. Phys. Lett.* **45**, 615 (1984).
63. A. J. Drehman and D. Turnbull, *Scr. Metall.* **15**, 543 (1981).
64. H. J. Leamy and A. G. Dirks, *J. Phys. D* **10**, L95 (1977).
65. T. Watanabe and T. Tanabe, *Mater. Sci. Eng.* **23**, 97 (1976).
66. A. Brenner, D. E. Couch, E. K. Williams, *J. Res. Natl. Bur. Stand.* **44**, 109 (1950).
67. S. Mørup and J. van Wonterghem, in *Proceedings of the Symposium on Magnetic Properties of Amorphous Metals*, A. Hernando, V. Madurga, M. C. Sanchez-Trujillo, M. Vasquez, Eds. (North-Holland, Amsterdam, 1987), pp. 1–5.
68. X. L. Yeh, K. Samwer, W. L. Johnson, *Appl. Phys. Lett.* **42**, 242 (1983).
69. M. Nastasi, D. Lilienfeld, H. H. Johnson, J. W. Mayer, *J. Appl. Phys.* **59**, 4011 (1986).
70. A. Dunlop and D. Lesueur, *Mater. Sci. Forum* **97–99**, 553 (1992).
71. D. E. Luzzi and M. Meshii, *J. Less-Common Met.* **140**, 193 (1988).
72. D. Lesueur, *Fizika* **2**, 13 (1970).
73. G. K. Hubler, I. L. Singer, C. R. Clayton, *Mater. Sci. Eng.* **19**, 203 (1985).
74. B. X. Liu, W. L. Johnson, M. A. Nicolet, *Appl. Phys. Lett.* **42**, 45 (1983).
75. R. B. Schwarz, R. R. Petrich, C. K. Saw, *J. Non-Cryst. Solids* **76**, 281 (1985).
76. C. C. Koch, O. B. Cavin, C. G. McKamey, J. O. Scarbrough, *Appl. Phys. Lett.* **43**, 1017 (1983).
77. S. Hasegawa and R. Ray, *J. Appl. Phys.* **49**, 4174 (1978).
78. B. G. Lewis and H. A. Davies, *Mater. Sci. Eng.* **23**, 179 (1976).
79. F. E. Luborsky, *ibid.* **28**, 139 (1977).
80. D. E. Polk and H. S. Chen, *J. Non-Cryst. Solids* **15**, 165 (1974).
81. A. Inoue and T. Masumoto, *Sci. Rep. Res. Inst. Tohoku Univ.* **28A**, 165 (1980).
82. M. Fischer, D. E. Polk, B. C. Giessen, in *Proceedings of the First International Conference on Rapid Solidification Processing*, R. Mehrabian, B. H. Kear, M. Cohen, Eds. (Claitor's, Baton Rouge, LA, 1978), p. 140.
83. R. C. Ruhl, B. C. Giessen, M. Cohen, N. J. Grant, *Acta Metall.* **15**, 1693 (1967).
84. R. Ray, B. C. Giessen, N. J. Grant, *Scr. Metall.* **2**, 359 (1968).
85. S. J. Poon and W. L. Carter, *Solid State Commun.* **35**, 249 (1980).
86. G. P. J. Gregan, Y. D. Dong, M. G. Scott, in *Proceedings of the International Conference on Metallic Glasses* (Kultura, Budapest, 1981), vol. 2, p. 197.
87. A. Inoue, T. Zhang, T. Masumoto, *Mater. Trans. J.I.M.* **31**, 177 (1990).
88. A. Inoue, K. Ohtera, T. Masumoto, *Jpn. J. Appl. Phys.* **27**, L736 (1988).
89. A. P. Tsai, A. Inoue, Y. Bizen, T. Masumoto, *Acta Metall.* **37**, 1443 (1989).
90. W. L. Johnson, S. J. Poon, P. Duwez, *Phys. Rev. B* **11**, 150 (1975).
91. K. H. J. Buschow, *J. Less-Common Met.* **66**, 89 (1979).
92. A. Inoue, T. Zhang, T. Masumoto, *Mater. Trans. J.I.M.* **30**, 965 (1989).
93. A. Calka *et al.*, *Scr. Metall.* **11**, 65 (1977).
94. F. Sommer, G. Duddek, B. Predel, *Z. Metallkd.* **69**, 587 (1978).
95. S. G. Kim, A. Inoue, T. Masumoto, *Mater. Trans. J.I.M.* **31**, 929 (1990).
96. S. Hasegawa and L. E. Tanner, *J. Appl. Phys.* **49**, 3211 (1977).
97. R. Ray and E. Musso, U.S. Patent 3 981 722 (1976).
98. H. G. Hillenbrand, E. Hornbogen, U. Köster, in *Proceedings of the Fourth International Conference on Rapidly Quenched Metals*, T. Masumoto and K. Suzuki, Eds. (JIM, Sendai, 1982), pp. 1369–1372.
99. W. L. Johnson, in *Glassy Metals I*, H. J. Güntherodt and H. Beck, Eds. (Springer, Berlin, 1981), pp. 191–223.
100. B. M. Clemens, W. L. Johnson, R. B. Schwarz, *J. Non-Cryst. Solids* **61&62**, 817 (1984).
101. K. Ohtera, A. Inoue, T. Terabayashi, H. Nagahama, T. Masumoto, *Mater. Trans. J.I.M.* **33**, 775 (1992).
102. Y. H. Kim, A. Inoue, T. Masumoto, *ibid.* **32**, 334 (1991).
103. M. F. Ashby, *Acta Metall.* **37**, 1273 (1989).

Hall and P. G. Wolynes, *J. Chem. Phys.* **86**, 2943 (1987).
110. H. Frauenfelder, S. G. Sligar, P. C. Wolynes, *Science* **254**, 1598 (1991).
111. W. Doster, A. Bachleitner, R. Dunau, M. Hiebi, E. Lüscher, *Biophys. J.* **50**, 213 (1986).
112. V. I. Goldanskii, Yu. F. Krupyanskii, V. N. Fleurov, *Dok. Akad. Nauk SSSR* **272**, 978 (1983).
113. F. Parak, J. Heidemeier, G. U. Nienhaus, *Hyperfine Interactions* **40**, 147 (1988).
114. W. Doster, S. Cusack, W. Petry, *Nature* **337**, 754 (1989).
115. B. F. Rasmussen, A. M. Stock, D. Ringe, G. A. Petsko, *Ibid.* **357**, 423 (1992).
116. K. Kuczera, J. Smith, M. Karplus, *Proc. Natl. Acad. Sci. U.S.A.* **87**, 1601 (1990).
117a.I. V. Sochava, G. I. Tseretoli, O. I. Smirnova, *Biofizika*, 36 (1991).
117b.I. V. Sochava and O. I. Smirnova, *Food Hydrocolloids* **6**, 513 (1993).
118. G. Sartor, A. Hallbrucker, K. Hofer, E. Mayer, *J. Phys. Chem.* **96**, 5133 (1992); G. Sartor, E. Mayer, G. P. Johari, *Biophys. J.* **66**, 249 (1994).
119. J. L. Green, J. Fan, C. A. Angell, *J. Phys. Chem.* **98**, 13780 (1994).
120. K. E. Prehoda and J. L. Markley, in *High Pressure Effects in Molecular Biophysics and Enzymology*, J. L. Markley, C. A. Royer, D. Northrop, Eds. (Oxford Univ. Press, New York, in press), any references cited therein, and J. L. Markley, private communication. Note the important reassessment of packing efficiencies of folded and unfolded states which is made in this study. While the unfolding transition may, like the melting of a small crystal, be a transition between two global minima for the individual molecules, the phenomenon observed in a protein solution is the consequence of this event for very many such molecules, and this has the character of a high positive entropy change, small (net) negative volume change, chemical conversion process.
121. V. N. Morozov and T. Ya Morozova, *J. Biomol. Struct. Dyn.* **11**, 459 (1993).
122. R. C. Hoseney, K. Zeleznak, C. S. Lai, *Cereal Chem.* **63**, 285 (1986).
123. A. Zipp and W. Kauzmann, *Biochemistry* **12**, 4217 (1973).
124. A. Petry *et al.*, *Phys. B. Condens. Mater.* **83**, 175 (1991).
125. B. Frick and D. Richter, *Phys. Rev. B* **47**, 14795 (1993).
126. B. Frick, D. Richter, W. Petry, U. Buchenau, *Z. Phys.* **B70**, 73 (1988).
127. A. Chahid, A. Alegria, J. Colmenero, *Macromolecules* **27**, 3282 (1994).
128. B. Frick and D. Richter, *Science* **267**, 1939 (1995).
129. U. Buchenau and R. Zorn, *Europhys. Lett.* **18**, 523 (1992).
130. J. Shao and C. A. Angell, unpublished results.
131. L. V. Woodcock, *Chem. Phys. Lett.* **10**, 257 (1971).
132. A. Rahman, R. H. Fowler, A. H. Narten, *J. Chem. Phys.* **57**, 3010 (1972).
133. J. Kieffer and C. A. Angell, *J. Non-Cryst. Solids* **106**, 336 (1988), and other references cited therein.
134. C. Boussard, G. Fontaneau, J. Lucas, *J. Non-Cryst. Solids*, in press.
135. R. J. Roe, *J. Chem. Phys.* **100**, 1612 (1994).
136. A. J. Martin and W. Brenig, *Phys. Status Solidi* **64**, 163 (1974).
137. E. Duval *et al.*, *Phys. Rev. Lett.* **56**, 2052 (1986); A. Boukeneter *et al.*, *ibid.* **57**, 2391 (1986); E. Duval *et al.*, *J. Phys. Condens. Mater.* **2**, 10227 (1990).
138. V. N. Novikov and A. P. Sokolov, *Solid State Commun.* **77**, 243 (1991); A. P. Sokolov, A. Kislink, M. Soltwisch, D. Quitmann, *Phys. Rev. Lett.* **69**, 1540 (1992).
139. L. Börjesson, A. K. Hassan, J. Swenson, L. M. Torell, *Phys. Rev. Lett.* **70**, 4027 (1993).
140. A. K. Hassan, L. Börjesson, L. M. Torell, *J. Non-Cryst. Solids* **172–174**, 154 (1994).
141. J. Colmenero, A. Arbe, A. Alegria, *Phys. Rev. Lett.* **71**, 2603 (1993).
142. K.-L. Ngai, *J. Chem. Phys.* **98**, 7588 (1993).
143. ———, in *Diffusion in Amorphous Solids*, H. Jain and D. Gupta, Eds. (The Minerals, Metals, and Materials Society, Warrendale, PA, 1994), p. 17.
144. M. H. Cohen and D. Turnbull, *J. Chem. Phys.* **34**, 120 (1960).
144. P. Harrowell, private communication.
145. T. Atake and C. A. Angell, *J. Phys. Chem.* **83**, 3218 (1979).
146. S. Cusack and W. Doster, *Biophys. J.* **58**, 243 (1990).
147. C. Herbst *et al.*, *J. Non-Cryst. Solids* **172–174**, 265 (1994).
148. L. Haar, J. Gallagher, G. Kell, *G.S. National Bureau of Standards-National Research Council Steam Tables* (McGraw-Hill, New York, 1985).
149. P. W. Anderson, in *Ill-Condensed Matter*, R. Ballian, R. Maynard, G. Toulouse, Eds. (North-Holland, Amsterdam, 1979), pp. 161–261.
150. A. L. Greer, *Science* **267**, 1947 (1995).
151. I would like to acknowledge the support of the NSF-DMR under Solid State Chemistry grant DMR9108028-002, and the help of many colleagues through stimulating discussions of this subject area. In particular, I am grateful to U. Buchenau, H. Frauenfelder, T. Grande, W. Kauzmann, W. Kob, P. Madden, J. Markley, P. McMillan, P. Poole, H. Sillescu, F. Sciortino, and G. Wolf.

A Topographic View of Supercooled Liquids and Glass Formation

Frank H. Stillinger

Various static and dynamic phenomena displayed by glass-forming liquids, particularly those near the so-called "fragile" limit, emerge as manifestations of the multidimensional complex topography of the collective potential energy function. These include non-Arrhenius viscosity and relaxation times, bifurcation between the α- and β-relaxation processes, and a breakdown of the Stokes-Einstein relation for self-diffusion. This multidimensional viewpoint also produces an extension of the venerable Lindemann melting criterion and provides a critical evaluation of the popular "ideal glass state" concept.

Methods for preparing amorphous solids include a wide range of techniques. One of the most prominent, both historically and in current practice, involves cooling a viscous liquid below its thermodynamic freezing point, through a metastable supercooled regime, and finally below a "glass transition" temperature T_g. A qualitative understanding, at the molecular level, has long been available for materials produced by this latter preparative sequence; however, many key aspects of a detailed quantitative description are still missing. Fortunately, focused and complimentary efforts in experiment, numerical simulation, and analytical theory currently are filling the gaps.

The present article sets forth a descriptive viewpoint that is particularly useful for discussing liquids and the glasses that can be formed from them, although in principle it applies to all condensed phases. Conceptual precursors to this viewpoint can be found throughout the scientific literature (*1*), but most notably in the work of Goldstein (*2*). The objective here is to classify and unify at least some of the many static and kinetic phenomena associated with the glass transition.

The author is at AT&T Bell Laboratories, Murray Hill, NJ 07974, USA.

Interaction Potentials

Condensed phases, whether liquid, glassy, or crystalline, owe their existence and measurable properties to the interactions between the constituent particles: atoms, ions, or molecules. These interactions are comprised in a potential energy function $\Phi(\mathbf{r}_1 \cdots \mathbf{r}_N)$ that depends on the spatial location $\mathbf{r}_i$ for each of those particles. The potential energy includes (as circumstances require) contributions from electrostatic multipoles and polarization effects, covalency and hydrogen bonding, short-range electron-cloud-overlap repulsions and longer range dispersion attractions, and intramolecular force fields. Obviously, the chemical characteristics of any substance of interest would substantially influence the details of Φ. Time evolution of the multiparticle system is controlled by the interactions, and for most applications of concern here the classical Newtonian equations of motion (incorporating forces specified by Φ) provide an adequate description of the particle dynamics.

In order to understand basic phenomena related to supercooling and glass formation, it is useful to adopt a "topographic" view of Φ. By analogy to topographic maps of the Earth's features, we can imagine a multidimensional topographic map showing the "elevation" Φ at any "location" $\mathbf{R} \equiv (\mathbf{r}_1 \cdots \mathbf{r}_N)$ in the configuration space of the N particle system. This simple change in perspective from conventional

three-dimen sional space to a space of much higher dimension [3N for structureless particles, and even more for particles that are asymmetric or nonrigid or both (3)] intrinsically creates no new information, but it facilitates the description and understanding of collective phenomena that operate in condensed phases, particularly in liquids and glasses.

An obvious set of topographic questions to ask concerns the extrema of the Φ surface, such as maxima ("mountain tops"), minima ("valley bottoms"), and saddle points ("mountain passes"). The minima correspond to mechanically stable arrangements of the N particles in space, with vanishing force and torque on every particle; any small displacement from such an arrangement gives rise to restoring forces to the undisplaced arrangement. The lowest lying minima are those whose neighborhoods would be selected for occupation by the system if it were cooled to absolute zero slowly enough to maintain thermal equilibrium; for a pure substance, this would correspond to a virtually perfect crystal. Higher lying minima correspond to amorphous particle packings and are sampled by the stable liquid phase above the melting temperature T_m (4).

Figure 1 shows a highly schematic illustration of the multidimensional "Φ-scape." Such a simplified representation can be misleading, but it serves to stress several key points. First, the minima have a substantial variation in depth and are arranged in a complex pattern throughout configuration space. Second, each minimum is enclosed in its own "basin of attraction," most simply defined as the set of all configurations in its "valley," that is, all locations that strict downhill motion would connect to that minimum. Third, contiguous basins share a boundary containing at least one saddle point, or transition state. Fourth, equivalent minima can be attained by permutations of identical particles. This last point implies, for a pure substance, that every minimum belongs to a group of $N!$ equivalent minima distributed regularly throughout the multidimensional configuration space.

An important issue concerning the Φ-scape topography that remains largely unresolved concerns the number of minima $\Omega(N)$, and in particular how fast it rises with N. Rather general arguments (bolstered by exact calculations for some special theoretical models) yield a simple generic form for the large-N limit in a single-component system (4, 5):

$$\Omega(N) \sim N! \exp(\alpha N) \qquad (1)$$

where $\alpha > 0$ depends significantly on the chemical nature of the substance considered. The permutational factor $N!$ has already been explained; the challenge is to predict α reliably from known molecular structures and interactions.

Melting and Freezing Criteria

The topographic view of the Φ-scape advocated above leads to a clean separation between the inherent structural aspects of the substance under consideration (that is, the classification of potential energy local minima), and the "vibrational" aspects that concern motions within and among the basins defined by those inherent structures. Such a separation leads naturally to a fresh examination of an old but very useful idea, namely, the Lindemann melting criterion for crystalline solids, first formulated in 1910 (6).

The Lindemann criterion concerns the dimensionless ratio, $\ell(T)$, of the root-mean-square (rms) vibrational displacement of particles from their nominal lattice positions, to the nearest-neighbor spacing a. It asserts that when temperature rise causes $\ell(T)$ to reach a characteristic instability value, melting occurs. X-ray and neutron diffraction experiments provide measurements of $\ell(T)$ (through the Debye-Waller factor) for a wide variety of real substances, and computer simulations can be used to calculate $\ell(T)$ for model systems. These results show that $\ell(T_m)$ varies a bit with crystal structure: It is approximately 0.13 for face-centered-cubic crystals and 0.18 for body-centered-cubic crystals (7). In any event, it is substantially constant across substances in a given crystal class and provides a good account of the pressure dependence of T_m for a given substance.

Vibrational motions contributing to $\ell(T_m)$ have a significant anharmonic character. But aside from a very small concentration of thermally created point defects in the crystal, these vibrations are confined to the basins surrounding the $N!$ absolute minima. At any temperature T, then, the Lindemann ratio for the crystal can be expressed:

$$\ell(T) = <(\Delta\mathbf{R})^2>^{1/2}/(Na) \qquad (2)$$

where $\Delta\mathbf{R}$ is the intrabasin vibrational displacement from the absolute minimum in the multidimensional configuration space, and the brackets denote a thermal average confined to that basin at temperature T.

Although it is not obvious in the usual way of presenting the Lindemann melting criterion, Eq. 2 has a straightforward extension to the liquid phase. One simply recognizes that the thermal average and the displacements refer to inherent structures of the amorphous packing and their associated Φ-scape basins that predominate after melting. The mean nearest-neighbor distance a for the liquid phase (obtained from the measured radial distribution function) typically is close to that of the unmelted crystal.

No laboratory experiment has yet been devised to measure $\ell(T)$ for liquids. Nevertheless, computer simulations for models of real substances can be designed to supply the needed information. Numerically, these simulations are required to generate a representative collection of system configurations for the temperature of interest and to evaluate the rms particle displacements that return each configuration to its corresponding inherent structure. Although only a small number of simulations of this kind have thus far been carried out (8), the main features of this extension are clear, and are summarized qualitatively in Fig. 2. The crystal and liquid $\ell(T)$ curves are distinct; both monotonically increase with T, with the curve for the liquid located well above that for the crystal. At the melting-freezing point, ℓ_{liq} is approximately three times that for the crystal; equivalently, the rms particle displacement is approximately one-half that of the nearest-neighbor spacing.

In its conventional form, the Lindemann criterion advances an asymmetric, one-

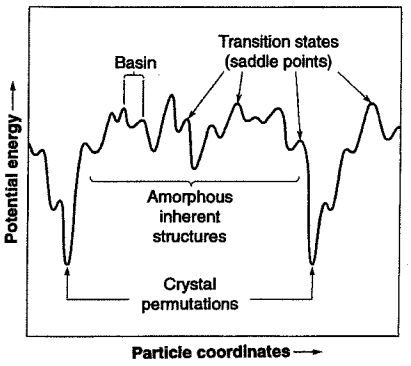

Fig. 1. Schematic diagram of the potential energy hypersurface in the multidimensional configuration space for a many-particle system.

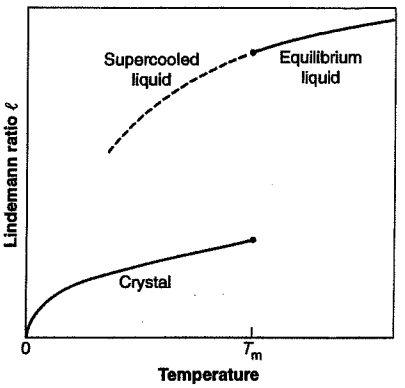

Fig. 2. Root-mean-square particle displacement divided by mean neighbor separation, versus temperature, for crystal and liquid phases. The value of this ratio for the crystal at the melting point, $\ell(T_m)$, is specified by the Lindemann melting criterion.

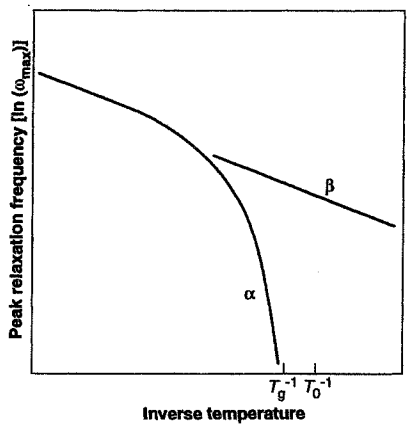

Fig. 3. Temperature dependence of peak relaxation (or absorption) frequencies for glass-forming liquids.

phase view of the first-order crystal-liquid transition. This model contrasts markedly with the thermodynamic description that calls for two-phase equality of pressure and chemical potential at the transition. However, the extension just described effectively restores two-phase symmetry. It supplements the melting criterion with an exactly analogous Lindemann-like freezing criterion for the liquid, specifically, that thermodynamic instability with respect to freezing occurs when cooling causes $\ell_{liq}(T)$ to decline to the cited transition value.

Although it is relatively difficult to superheat crystals above their T_m, supercooling of the melt is commonplace, particularly with viscous liquids. Figure 2 shows the extension of $\ell_{liq}(T)$ into the $T < T_m$ regime of supercooling, under the assumption that crystal nucleation has been avoided. In this extension, the system's configuration point $\mathbf{R}(t)$ continues to wander as time t progresses among the basins for amorphous inherent structures, without discovering entrance channels to any of the absolute-minimum basins of the crystalline state. Upon cooling to absolute zero, the system becomes trapped almost at random in one of these inherent-structure basins of the amorphous state, ℓ_{liq} becomes small (vanishing for classical statistics), and the system becomes a rigid glass.

Arrested Kinetics

The entire collection of $\Omega(N)$ basins can be classified by their depths. Let $\phi \equiv \Phi/N$ denote the inherent-structure potential energy for any given basin on a per-particle basis. In analogy to Eq. 1 above, it can be shown that the distribution of basins by depth has the form $N!\exp[\sigma(\phi)N]$ in the large-N limit (5). A mean vibrational free energy per particle, f_v, can then be defined for basins of depth ϕ. The equilibrium state of the system at temperature T corresponds to preferential occupation of basins with depth $\phi^*(T)$, which is the ϕ value that maximizes the simple combination (5, 9):

$$\sigma(\phi) - (k_B T)^{-1}[\phi + f_v(\phi,T)] \quad (3)$$

where k_B is Boltzmann's constant. When T is near T_m, this combination has two local maxima with respect to ϕ; the first-order melting transition corresponds to a discontinuous change in ϕ^* as the role of the absolute maximum switches from one to the other at T_m.

Supercooling the liquid phase below T_m kinetically avoids switching back to deep crystalline basins, but rather the liquid remains in those that correspond to the other local maximum of Eq. 3, given by $\phi^*_{liq}(T)$, that continues to refer to higher lying amorphous inherent structures. So long as the system configuration point $\mathbf{R}(T)$ can move more or less freely among the higher lying amorphous inherent structures and attain a representative sampling while avoiding crystal nucleation, the system remains in a reproducible quasi-equilibrium state of liquid supercooling (9).

The individual transitions that carry the system between contiguous (boundary-sharing) basins apparently almost always involve localized particle rearrangements. In other words, only order O(1) out of N of the particles undergo substantial location shifts. This is true whether the basins are those for substantially crystalline inherent structures (and the transition involves creation or destruction of point defects), or whether they refer to a pair of amorphous packings. Consequently, the activation barrier that must be surmounted, and the final change in basin depth will also only be O(1). Because the total kinetic energy is much larger (roughly Nk_BT), enough thermal energy is virtually always available in principle to surmount the intervening barrier. The bottleneck is that this kinetic energy is distributed throughout the many-particle system, and it may take a very long time for a proper fluctuation to concentrate enough kinetic energy at the required location to effect the transition between basins.

Relaxation response functions in the time domain, $g_v(t)$, to any of a variety of weak external perturbations v (mechanical, electrical, thermal, optical, and so forth) provide an indication of the actual restructuring kinetics resulting from interbasin transitions. If the assumption that the initial-time normalization $g_v(0) = 1$ is imposed, the areas under the $g_v(t)$ curve along the positive time axis define mean relaxation times $\tau_v(T)$. These depend somewhat on property v, but in supercooled liquids they tend to display essentially a common rapid rise with declining temperature and can often be fitted to a Vogel-Tammann-Fulcher (VTF) form (10):

$$\tau_v(T) \cong \tau_0 \exp[A/(T - T_0)] \quad (4)$$

where τ_0 is in the picosecond range and A and T_0 are positive constants.

So long as all τ_v are substantially shorter than the time available for experimental measurement, the supercooled liquid remains in a state of quasi-equilibrium, and in particular inhabits and moves among basins whose depths are closely clustered around $\phi^*_{liq}(T)$. But as T declines, the mean relaxation times represented by the VTF form increase strongly and all cross the time scale of experimental measurement at essentially a common glass transition temperature $T_g > T_0$. Further reduction in T fails to lower the depth of the inhabited basins below $\phi^*_{liq}(T_g)$. The supercooled liquid then has fallen out of quasi-equilibrium. The ratio T_g/T_m for most good glass-forming liquids falls in the range from 0.60 to 0.75.

Careful examination of the relaxation functions $g_v(t)$ above T_g reveals the presence of distinct processes. At very short times (comparable to vibrational periods), intrabasin relaxation predominates. This domain is followed by a much more extended time regime during which interbasin structural relaxation processes occur, and in the long-time limit of this regime the relaxation inevitably seems to display a Kohlrausch-Williams-Watts (KWW) "stretched exponential" decay (11):

$$g_v(t) \sim \Gamma_v \exp[-(t/t_v)^\theta] \quad (5)$$

in which $0 < \theta \leq 1$ and Γ_v is a constant; the characteristic time t_v is comparable to mean relaxation time τ_v when T is near T_g.

The $\theta = 1$ limit in Eq. 5 corresponds to simple Debye relaxation, with t_v serving as the single structural relaxation time. However, smaller θ values lead to a broad distribution of relaxation times, and by transforming g_v to the frequency domain this breadth becomes explicit (12). Peaks in the frequency-dependent absorption then correspond approximately to the dominant relaxation times.

As Fig. 3 illustrates, the temperature dependence of peak relaxation frequency for liquids often exhibits a bifurcation (13). In the equilibrium liquid range and into the moderately supercooled regime, there is a single absorption maximum frequency. Upon approaching T_g, this peak splits into a pair of maxima, the slow α ("primary") and faster β ("secondary") relaxations. The former are non-Arrhenius and kinetically frozen out at T_g, and the latter are more nearly Arrhenius and remain operative at T_g.

The α, β relaxation bifurcation has a straightforward interpretation in terms of the Φ topography. As T declines, the configuration point $\mathbf{R}(t)$ is forced into regions of increasingly rugged and heterogeneous

topography in order to seek out the ever deeper basins that are identified by $\phi^*_{liq}(T)$. The lower the temperature, the rarer and more widely separated these basins must be. However, the elementary transition processes that connect contiguous basins continue to require only local rearrangements of small numbers of particles. Evidently, the basins are geometrically organized to create a two-scale length and potential energy pattern; Fig. 4 illustrates this feature.

The β processes are identified with the elementary relaxations between neighboring basins, whereas the α processes entail escape from one deep basin within a large-scale "crater" or "metabasin" and eventually into another (*14*). Because the latter requires a lengthy directed sequence of elementary transitions, it will acquire a net elevation change (activation energy) many times that of the former. Also, the vast intervening stretch of higher lying basins produces a large activation entropy.

Viscosity and Self-Diffusion

The relaxational response of a fluid to shear stress is often described by a specific instance of Eq. 4, the Maxwell relaxation time $\tau_M(T)$, defined by the ratio of the shear viscosity $\eta(T)$ to the elastic modulus G, which is nearly temperature independent. Consequently, the VTF form in Eq. 4 is also a useful representation of shear viscosity [indeed, this was its original application (*10*)]:

$$\eta(T) \cong \eta_0 \exp[B/(T - T_0)] \qquad (6)$$

with virtually the same divergence temperature T_0 that obtains for other types of relaxation. Experimentally, T_g's often correspond to η in the range from 10^{11} to 10^{13} poise for nonpolymeric liquids.

The VTF representation for viscosity generates a useful classification of glass-forming liquids between "strong" and "fragile" extremes (*15*), depending on the value of the ratio T_0/T_m (or alternatively T_0/T_g). The strong limit has $T_0/T_m \cong 0$, and $\eta(T)$ displays Arrhenius temperature behavior; real material examples that appear to be close to this limit are the oxide glasses SiO_2 and GeO_2. The fragile limit displays dramatic non-Arrhenius $\eta(T)$, and is illustrated by orthoterphenyl, and the ionic material $K_{0.6}Ca_{0.4}(NO_3)_{1.4}$.

The variation in behavior between the strong and fragile extremes can be traced back to topographic differences in the Φ-scapes for the respective materials. The extreme limit of strong glass formers presents a uniformly rough (single energy scale) topography, in which only the β transitions of Fig. 4 have relevance. Little or no coherent organization of the individual basins into large and deep craters, associated with the low-temperature α transitions, appears to be

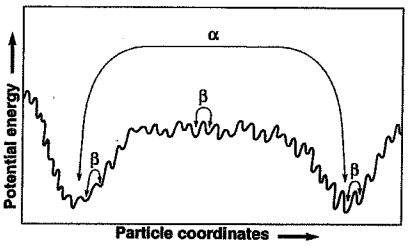

Fig. 4. Two-scale potential energy topography characteristic of regions of configuration space explored by fragile glass formers near T_g. The elementary interbasin transitions are associated with β relaxations, and large distance intercrater transitions are associated with α relaxations.

present. It is no surprise then that the α,β bifurcation is weak or absent in the strong cases. In contrast, the most fragile glass formers indeed exhibit significant Φ-scape cratering and distinctive α,β bifurcation. The relatively large effective singularity temperature T_0 for fragile materials reflects the larger and wider net barriers that they must surmount, as T declines toward T_0, for the system configuration to pass from the interior of one inhabited crater to another of comparable or greater depth.

The self-diffusion constant D measures the rate of increase with time, because of Brownian motion, of the mean square displacement of a tagged particle in the medium. The Stokes-Einstein relation connects D to η and to an effective hydrodynamic radius b for the particle:

$$D(T) = k_B T/[6\pi b\eta(T)] \qquad (7)$$

(the constant 6π assumes a "sticking" boundary condition at the particle surface). This relation has been remarkably successful at correlating independent measurements of $D(T)$ and $\eta(T)$ for many liquids as both vary over many orders of magnitude in the stable and supercooled liquid regimes. However, some recent experiments on fragile glass formers near T_g show a striking breakdown of Eq. 7; in these cases $D(T)$ becomes two orders of magnitude or more larger than the measured $\eta(T)$ would indicate (*16*). Paradoxically, this dramatic effect occurs while the corresponding rotational diffusion rate is still linked to $\eta(T)$ or only weakly decoupled (*17*).

Once again, the Φ-scape cratering characteristic for fragile glass formers offers an explanation. When the temperature is low and the system configuration point emerges from one deep crater to search for another, it has been emphasized that a long sequence of elementary interbasin transitions will be involved. In three dimensions, this sequence would appear as a local structural excitation running around in a microscopic domain that encompasses many particles, temporarily fluidizing that domain compared to the surroundings. Because such domains are expected to be large on the molecular scale near T_g and to have long lifetimes, translational diffusion receives a disproportionate enhancement compared to rotational diffusion, and a detailed analysis (*18*) shows that the latter continues to adhere more closely than the former to the temperature dependence of $\eta(T)$.

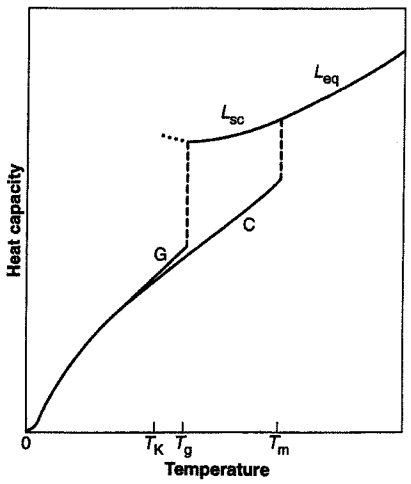

Fig. 5. Typical heat capacity curves for fragile glass formers in crystal (C), supercooled liquid (L_{sc}), equilibrium liquid (L_{eq}), and glass (G) phases; T_K is the Kauzmann temperature.

Ideal Glass State?

Figure 5 illustrates schematically variation with temperature of the heat capacity (C_p, constant pressure) typically observed for fragile glass formers. Notable features are: (i) C_p rises discontinuously when the crystal melts at T_m; (ii) supercooling the liquid down toward T_g increases the discrepancy between C_p (liquid) and C_p (crystal); and (iii) further cooling produces a nearly discontinuous drop in C_p (liquid) so that C_p (glass) is very close to that of C_p (crystal) at the same low temperature. In view of the basin-trapping interpretation of the glass transition, it can be concluded that the intrabasin vibrational properties are largely the same for all basins, whether corresponding to crystalline or to amorphous inherent structures. Furthermore, most of the enhancement of C_p (liquid) over C_p (crystal) above T_g stems from the temperature variation of ϕ^*_{liq}, the depth of the basins predominately inhabited by the supercooled liquid.

The latent heat of melting causes the liquid at T_m to possess a substantially higher entropy than the crystal. However, the C_p discrepancy illustrated in Fig. 5 means that the liquid loses entropy faster than the crystal as both are cooled below T_m. The strongly supercooled liquid at T_g still has the higher

entropy, although the difference has been substantially reduced. Smooth extrapolation of C_p (liquid) below T_g and of the corresponding entropy indicate the existence of a positive "Kauzmann temperature" T_K at which the crystal and the extrapolated liquid attain equal entropies (*19*). Considering that vibrational entropies are nearly the same for the two phases, and that the inherent structural entropy of the ordered crystal vanishes, the fully relaxed glass at T_K (the extrapolated liquid) must also have vanishing inherent structural entropy. This realization, coupled with the empirical observation that $T_K \cong T_0$, the mean relaxation-time divergence temperature, has generated the concept of an "ideal glass state" that could be experimentally attained if only sufficiently slow cooling rates were available (*20*).

If indeed it exists, the ideal glass state must correspond to the inherent structure with the lowest potential energy (deepest "crater") that is devoid of substantial regions with local crystalline order. Unfortunately, the details of this noncrystallinity constraint are unclear but may be crucial: Qualifying inherent structures may depend on the maximum size and degree of perfection permitted crystalline inclusions in otherwise amorphous structures. This ambiguity, or non-uniqueness of choice criterion, would seem to undermine the concept of a substantially unique ideal glass state.

It has also been argued (*9*) that the seemingly innocuous extrapolations that identify a positive Kauzmann temperature T_K (and by implication T_0) are flawed. Localized particle rearrangements (associated with β relaxations) are always possible, even in a hypothetical ideal glass structure, and raise the potential energy only by O(1). These structural excitations in the strict sense prevent attaining the ideal glass state at positive temperature, in conflict with the usual view (*20*).

In spite of these formal reservations, the ideal glass state concept remains valuable. Careful and systematic experiments on the most fragile glass formers should help to remove some of the obscuring uncertainties.

Conclusions

By focusing attention on the topographic characteristics of Φ in the multidimensional configuration space, a comprehensive description becomes available for static and kinetic phenomena exhibited by supercooled liquids and their glass transitions. In particular, this viewpoint rationalizes the characteristic properties of fragile glass formers, including non-Arrhenius viscosity, primary-secondary relaxation bifurcation, and the enhancement of self-diffusion rates over the Stokes-Einstein prediction. This multidimensional topographic representation has the further benefit of uncovering and promoting several basic research topics that need sustained experimental and theoretical-simulational attention. Examples of the latter are the material-specific enumeration of inherent structures (Φ minima), the exploitation of the Lindemann-like freezing criterion for liquids and its relation to the glass transition, and the critical evaluation of the ideal-glass-state concept.

REFERENCES AND NOTES

1. J. D. Bernal, *Nature* **183**, 141 (1959); H. Eyring *et al.*, *Proc. Natl. Acad. Sci. U.S.A.* **44**, 683 (1958); M. R. Hoare, *Adv. Chem. Phys.* **40**, 49 (1979).
2. M. Goldstein, *J. Chem. Phys.* **51**, 3728 (1969); *ibid.* **67**, 2246 (1977).
3. For constant-pressure circumstances, system volume becomes an additional coordinate and Φ includes a pressure-volume contribution *PV*.
4. F. H. Stillinger and T. A. Weber, *Science* **225**, 983 (1984).
5. ———, *Phys. Rev. A* **25**, 978 (1982).
6. F. A. Lindemann, *Z. Phys.* **11**, 609 (1910).
7. H. Löwen, *Phys. Rep.* **237**, 249 (1994).
8. R. A. LaViolette and F. H. Stillinger, *J. Chem. Phys.* **83**, 4079 (1985).
9. F. H. Stillinger, *ibid.* **88**, 7818 (1988).
10. G. W. Scherer, *J. Am. Ceram. Soc.* **75**, 1060 (1992).
11. K. L. Ngai, Comments *Solid State Phys.* **9**, 127 and 141 (1979); R. Böhmer, K. L. Ngai, C. A. Angell, D. J. Plazek, *J. Chem. Phys.* **99**, 4201 (1993).
12. E. W. Montroll and J. T. Bendler, *J. Stat. Phys.* **34**, 129 (1984).
13. G. P. Johari and M. Goldstein, *J. Chem. Phys.* **53**, 2372 (1970).
14. F. H. Stillinger, *Phys. Rev. B* **41**, 2409 (1990).
15. C. A. Angell, in *Relaxations in Complex Systems*, K. Ngai and G. B. Wright, Eds. (National Technical Information Service, U.S. Department of Commerce, Springfield, VA, 1985), p. 1.
16. F. Fujara, B. Geil, H. Sillescu, G. Fleischer, *Z. Phys. B* **88**, 195 (1992); M. T. Cicerone and M. D. Ediger, *J. Phys. Chem.* **97**, 10489 (1993); R. Kind *et al.*, *Phys. Rev. B* **45**, 7697 (1992).
17. M. T. Cicerone, F. R. Blackburn, M. D. Ediger, *J. Chem. Phys.* **102**, 471 (1995).
18. F. H. Stillinger and J. A. Hodgdon, *Phys. Rev. E* **50**, 2064 (1994).
19. W. Kauzmann, *Chem. Rev.* **43**, 219 (1948).
20. J. Jäckle, *Rep. Prog. Phys.* **49**, 171 (1986).

The Microscopic Basis of the Glass Transition in Polymers from Neutron Scattering Studies

B. Frick* and D. Richter

Recent neutron scattering experiments on the microscopic dynamics of polymers below and above the glass transition temperature T_g are reviewed. The results presented cover different dynamic processes appearing in glasses: local motions, vibrations, and different relaxation processes such as α- and β-relaxation. For the α-relaxation, which occurs above T_g, it is possible to extend the time-temperature superposition principle, which is valid for polymers on a macroscopic scale, to the microscopic time scale. However, this principle is not applicable for temperatures approaching T_g. Below T_g, an inelastic excitation at a frequency of some hundred gigahertz (on the order of several wave numbers), the "boson peak," survives from a quasi-elastic overdamped scattering law at high temperatures. The connection between this boson peak and the fast dynamic process appearing near T_g is discussed.

Polymers have a very wide range of applicability and can be used in the solid, rubbery, or molten states. Solid polymers are used whenever elastic strength is required, and melts are used whenever viscous properties are desired. The intermediate range of viscoelasticity has particularly interesting properties and covers an especially wide temperature range for polymers because of their chain structure. Ideally, an understanding of the microscopic dynamics would be a prerequisite for optimized application. The limiting cases of the elastic solid and the viscous liquid are better understood than the viscoelastic regime, although a large amount of experimental data exists for the viscoelastic state (*1*). Polymers are generally amorphous solids, that is, they are microscopically disordered without translational symmetry and crystallization is rare. The microscopic disorder remains essentially unchanged as the polymer transforms from the glassy solid state to the melt or liquid state (Fig. 1A).

The key to understanding the property changes is the change of the microscopic dynamics, and any structural changes are therefore a consequence of it. Microscopically, elastic solids are characterized by their atoms or molecules being bound within a potential defined by the surrounding atoms.

B. Frick is in the Institut Laue-Langevin, BP156, F-38042 Grenoble Cedex 9, France. D. Richter is in the Institut für Festkörperforschung, Forschungsanlage Jülich, D-52425 Jülich, Germany.

*To whom correspondence should be addressed.